www.sciencemag.org/cgi/content/full/science.1218835/DC1

Supplementary Materials for

A Single Progenitor Population Switches Behavior to Maintain and Repair Esophageal Epithelium

David P. Doupé, Maria P. Alcolea, Amit Roshan, Gen Zhang,
Allon M. Klein, Benjamin D. Simons, Philip H. Jones*

*To whom correspondence should be addressed. E-mail: phj20@cam.ac.uk

Published 19 July 2012 on *Science* Express
DOI: 10.1126/science.1218835

This PDF file includes:

Methods

Animals

Adult mice doubly transgenic for the inducible *cre* allele AhcreERT and the conditional reporter allele of EYFP targeted to the Rosa 26 locus (Ahcre^{ERT}R26$^{flEYFP/wt}$) were generated as described *(12, 13).* In these mice, transcription of the cre mutant estrogen receptor fusion protein (creERT) is induced by ß-napthoflavone. Tamoxifen is also required for creERT to gain access to the nucleus and excise the loxP flanked "STOP" cassette resulting in EYFP expressionEYFP expression was induced in animals aged 8-12 weeks by an intraperitoneal dose of 80mg/kg β-napthoflavone and 1mg Tamoxifen *(18)*. For label retaining studies, Rosa26^{M2rtTA}/TetO-HGFP mice doubly transgenic for a reverse tetracycline-controlled transactivator (rtTA-M2) targeted to the Rosa 26 locus and a HIST1H2BJ/EGFP fusion protein (HGFP) expressed from a tetracycline promoter element were used *(1,14 and 15)*. HGFP expression was induced by treatment with doxycycline (DOX, 2mg/ml in drinking water sweetened with sucrose) for 4 weeks, after which DOX was withdrawn for two and four weeks in order to chase HGFP dilution *(1,14 and 15)* . Cohorts of three animals per time point were culled and esophagus and tail epidermis taken for analysis. Visualization of *Lgr5* transcription was achieved by using the *Lgr5*$^{EGFP\text{-}IRES\text{-}CreERT2/+}$ reporter mouse, in which EGFP was targeted to the 3' untranslated region of the *Lgr5* gene *(3)*. All experiments were conducted according to Home Office project licenses PPL80/2056 and PPL22/2282.

Immunostaining

Wholemounts from the middle third of esophageal epithelium and tail skin were prepared by cutting tissue into rectangular pieces of approximately 5 by 8mm and incubating for 2-3 hours in 5mM EDTA at 37ºC. The epithelium was then carefully peeled away from underlying tissue with fine forceps and fixed in 4% paraformaldehyde (PFA) in PBS for 15-25 minutes. For staining, wholemounts were blocked for 1 hour in staining buffer (0.5% Bovine Serum Albumin, 0.25% Fish skin gelatin, and 0.5% Triton X-100 in PBS) with 10% donkey or goat serum, according to the secondary antibody used. Primary and secondary antibodies were incubated in staining buffer overnight, followed by washing for 2 hours with 0.2% Tween-20 in PBS. Cryosections of 10µm thickness were fixed with 4% PFA for 5 minutes. EdU incorporation was detected with a Click-iT® chemistry kit according to the manufacturer's instructions (Invitrogen). When EdU staining was combined with immunofluorescent staining, the Click-labeling reaction was performed between primary and secondary antibody incubation. Please refer to Table S1 for a list of antibodies used in immunofluorescence. Confocal images were acquired on Zeiss LSM 510 META, Nikon ECLIPSE TE2000-U and Leica TCS SP5 II confocal microscopes and reconstructed using Volocity 5 image processing software (Improvision).

Esophageal endoscopy and biopsy

Mice undergoing endoscopy had anesthesia using a 100mg/kg Ketamine (Pfizer Animal Health) and 10mg/kg Xylazine (Bayer HealthCare AG) combination administered intraperitoneally. A 9.5Fr 30° forward oblique diagnostic miniature endoscope with a 3Fr instrument channel was used in conjunction with an AIDA COM II image capture system for high definition video recording (Karl Storz GmBH). Cannulation of the mouse esophagus was done under direct visualization up to a distance of 1.5-2cm from the vocal chords. 3Fr diameter biopsy forceps with double action jaws (Karl Storz GmBH) were used to create

superficial wounds in the middle third of the mouse esophagus of between 0.4 – 0.9mm diameter. Anesthesia was reversed using Atipamezole (Pfizer Animal Health) given at 1mg/kg subcutaneously at least 20 minutes after induction. Post-procedure, animals were maintained on a soft mashed diet and euthanized at appropriate timepoints mentioned in the text.

Dilution of Histone 2B-EGFP (HGFP) protein in esophageal epithelium (EE) in Rosa26^{M2rtTA}/TetO-HGFP mice

To quantify the intensity of HGFP fluorescence in EE from Rosa26^{M2rtTA}/ TetO-HGFP mice, samples were analyzed at time 0 (immediately after 4 weeks DOX treatment) and two weeks later. Unstained wholemounts from the middle third of the esophagus were imaged on a Leica TCS SP5 II confocal microscope using identical settings for all samples. Single 2μm slice images of the basal layer were analyzed for quantitative assessment of HGFP fluorescence in each independent cell by using Volocity 5 (Improvision).

Flow cytometric analysis

Esophagi from 3-5 adult mice (C57/Bl6; 2-3 month old) per sample were pooled, opened longitudinally, washed in PBS and treated with 0.5mg/ml thermolysin (Sigma) for 30 minutes at 37°C. The epithelium was then carefully peeled away from underlying tissue with fine forceps and washed in PBS to remove any contaminants. Epithelial sheets were then thoroughly minced and single-cell suspension obtained by non-enzymatic tissue dissociation using gentleMACS™ Dissociator (Miltenyi Biotec) followed by filtration through a 30μm cell strainer. Cells were centrifuged and resuspended in 1% fetal bovine serum in PBS. Staining with primary antibodies and/or isotype controls (5μg/ml) was performed for 30 minutes at 4°C. The following immunoglobulins were used for FACS at (1:100): FITC Rat anti-Mouse CD34 (RAM34; #553733) and FITC Rat IgG2a,κ isotype control (#553929) both from BD Pharmingen; Alexa Fluor® 647 Hamster anti-Mouse/Rat CD29 (HMβ1-1; #102214) and Alexa Fluor® 647 Hamster IgG isotype control (#400924) both from Biolegend. Incorporation of 7AAD (2μg/ml) was used to determine the cell viability.

Samples were analyzed on a MoFlow cell sorter (Dako Cytomation) and FlowJo FACS software (v7/9; Tree Star, Inc). 45,000 viable single cells were acquired for analysis. Isotype controls were used to exclude unspecific immunoglobulin binding. Surface expression of CD29 was used to identify basal cells. A population of doubly positive cells for CD34/CD29 could not be identified when compared to fluorescence minus one control for FITC (CD34/7AAD/CD29 was compared to FITC isotype/7AAD/CD29). Results were reproduced in each of 3 independent experiments.

Activated Caspase-3 staining

Wild type mice esophagi were cut into 10 μm cryosections. Immunostaining was performed as described. Fluorescent images were collected on a Zeiss Observer D1 microscope. 20 sections were analyzed for each mouse (3 in total), containing a total of 30000 basal cells. A positive control for the staining was obtained by irradiating a fresh esophageal sample with UVC and maintaining it in explant culture for 24 hours prior to sectioning *(18)*.

Parameters measured to determine homeostasis

Wholemounts from the middle third of the oesophagus were stained with DAPI and the basal cell marker keratin14, and Z stack images acquired by confocal microscopy. Images were viewed in Volocity software (Improvision). DAPI staining was used to score the number of basal cells per unit area and mitotic index, and Ki67 positive basal cells were scored from confocal images: 10 fields containing at least 2000 cells were scored for each mouse. The basal:suprabasal cell ratio was determined from Z stacks encompassing the basal layer and all nucleated suprabasal cells. The ratio of keratin 14 positive basal cells to nucleated, DAPI positive, suprabasal cells was scored using Volocity in at least three Z stacks per mouse.

Representativeness of labeling

Z stack images of clones one year post-induction were visualized by anti-GFP immunostaining. To assess proliferation in clones and surrounding unlabelled cells, we co-stained for either Ki-67 or Geminin, a protein expressed solely from S phase to early mitosis, using an anti-Geminin antibody that gives no staining in Geminin null embryos *(29)*. The basal: nucleated suprabasal cell ratio and the number of basal cells/unit area were scored in 138 clones and compared with the ratio in unlabelled cells measured as above.

Explant cultures

In order to study esophageal epithelial regrowth without the influence of the immune system, we developed a novel explant technique. Esophageal submucosa from wild type C57/Bl6 mice is dissected away from both the mucosa and muscle layers after 2 hour incubation with 5mM EDTA at 37ºC. The obtained submucosa is then cut in 5mm x 10 mm pieces and placed in transparent tissue culture inserts of 0.4 microns pore size (Greiner Bio-one). Immediately afterwards, two strips of esophageal epithelium (5 x 1 mm) from 7 days induced AhcreERTR26flEYFP/wt mice were placed on top of the submucosa. The mounted explants were left for 5 minutes to settle at 37ºC, and then covered with minimal medium containing: 1 part DMEM, 1 part Ham's F12, 10% fetal calf serum, 0.18 mM adenine, 5 µg/ml transferrin, 100 U/ml penicillin, 100 µg/ml streptomycin, 1.25ng/ml amphoteracin. The epithelium was cultured for 15 days at 37ºC and 5% CO_2, replacing the medium on alternate days. During this time new epithelium grows over the submucosa developing a new epithelial sheet. The new epithelium was either cryosectioned or wholemounted by peeling it away from the submucosa in a similar manner to the esophageal samples described above.

Statistical AnalysisThe methods used to analyze the cell lineage tracing experiments in $Ahcre^{ERT}R26^{flEYFP/wt}$ mice are set out in supplementary methods: theory.

Fig. S1

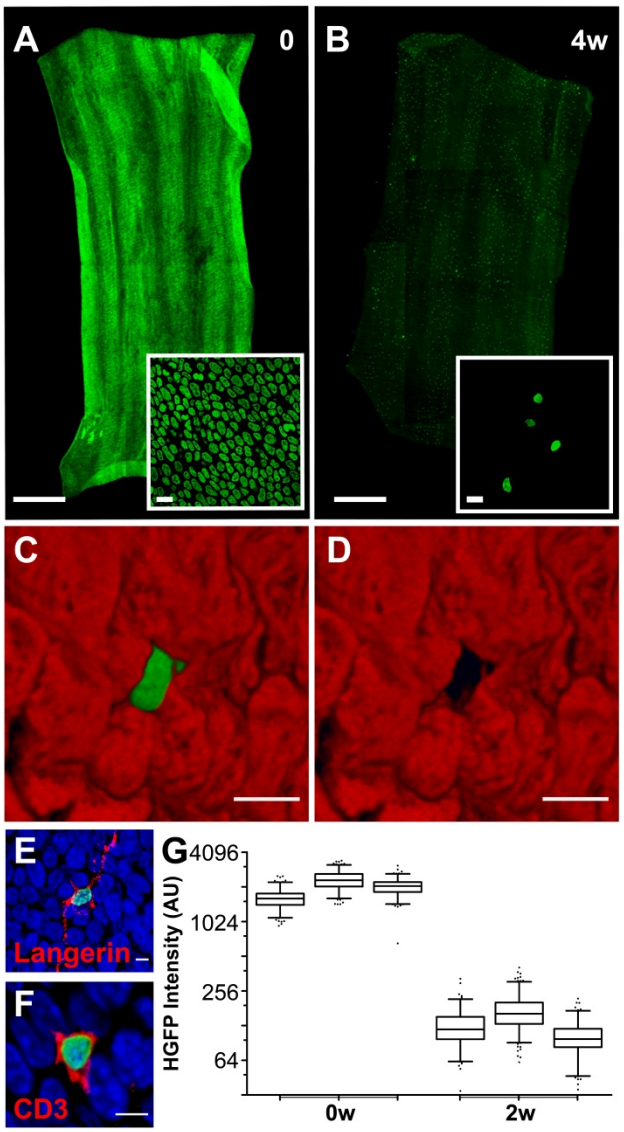

Dilution of Histone 2B-EGFP (HGFP) protein in esophageal epithelium (EE) in Rosa26^{M2rtTA}/TetO-HGFP mice and immunostaining of HGFP label retaining cells.

HGFP dilution in EE. Rosa26^{M2rtTA}/TetO-HGFP mice were treated with doxycycline (DOX) for 4 weeks, after which DOX was withdrawn and animals culled immediately (time 0) and 4 weeks later (4w) (Fig. 1C).

A, B: Wholemounts of EE were immunostained for GFP (green). At time 0, HGFP is expressed throughout the epithelium, whilst scattered HGFP retaining cells are seen at 4w. Scale bars: Main panels 500µm, insets10µm.
C - F: Rendered confocal z stacks of EE basal layer showing label retaining cells (green) at 4w are negative for Keratin 14 (red, C, D), but positive for CD45 (Fig. 1E inset), comprising Langerin positive Langerhan's cells (E) and CD3 positive lymphocytes (F). Scale bars 5µm.
G: Quantification of HGFP dilution. Box plots show median (central line), 25th and 75th percentile (box), 2.5th and 97.5th percentile (whiskers) and outliers (dots) for three mice at times indicated. AU, arbitrary units.

Fig. S2

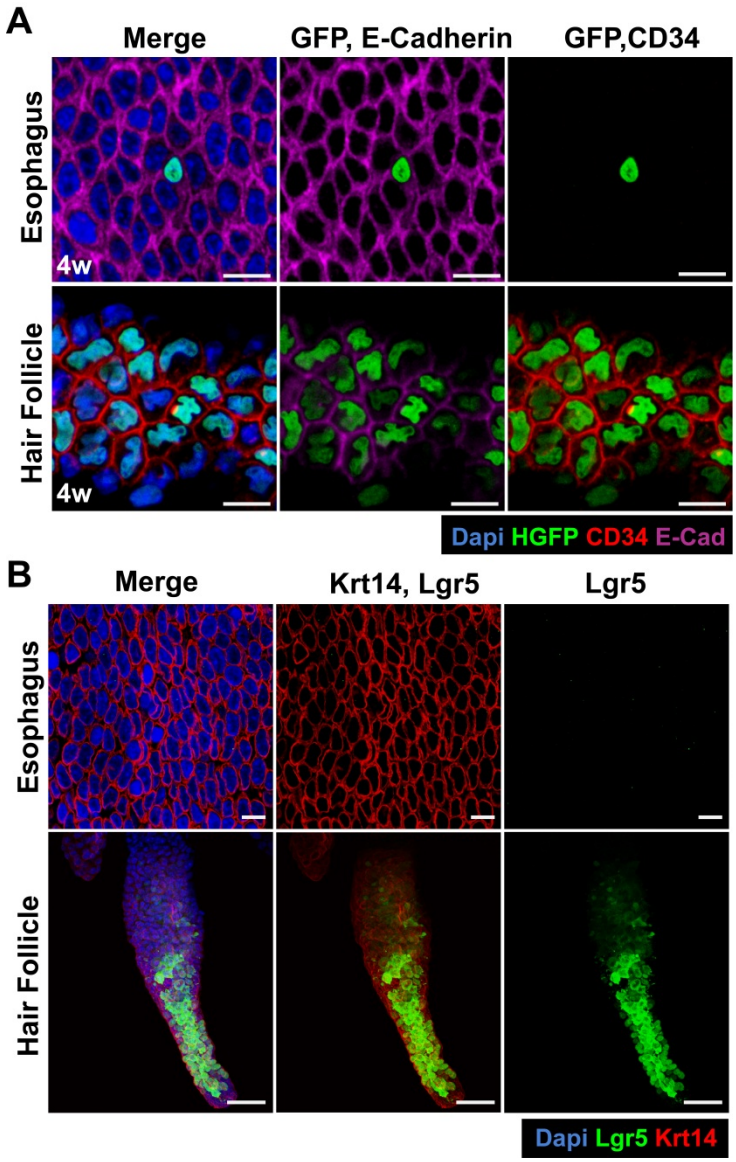

Histone 2B-EGFP (HGFP) retaining cells in EE do not express CD34 or Lgr5.

A: CD34 immunostaining in HGFP retaining cells in Rosa26^{M2rtTA}/TetO-HGFP mice treated with doxycycline (DOX) for 4 weeks, after which DOX was withdrawn and animals culled 4 weeks later (4w, Fig. 1C). Wholemounts of EE and epidermis were immunostained for HGFP (green), CD34 (red), the epithelial cell marker E Cadherin (purple) and DAPI (blue). CD34 is expressed by HGFP retaining cells in the hair follicle bulge *(1)*, but was undetectable in the HGFP retaining cells in the EE from the same animals. Scale bar 10μm.
B: *Lgr5* expression in EE. Esophageal and epidermal wholemounts were prepared from Lgr5$^{EGFP\text{-}IRES\text{-}CreERT2/+}$ mice in which EGFP, targeted to the 3' untranslated region of the *Lgr5* gene, reports *Lgr5* transcription (3). Cells in the hair follicle express EGFP, as previously reported, but no EGFP expression is detected in EE (*5*). *Lgr5* transcription is revealed by GFP staining, green, Keratin14 (Krt14) is red and Dapi is blue. Scale bars: Esophagus 10μm, Epidermis 50μm.

Fig. S3

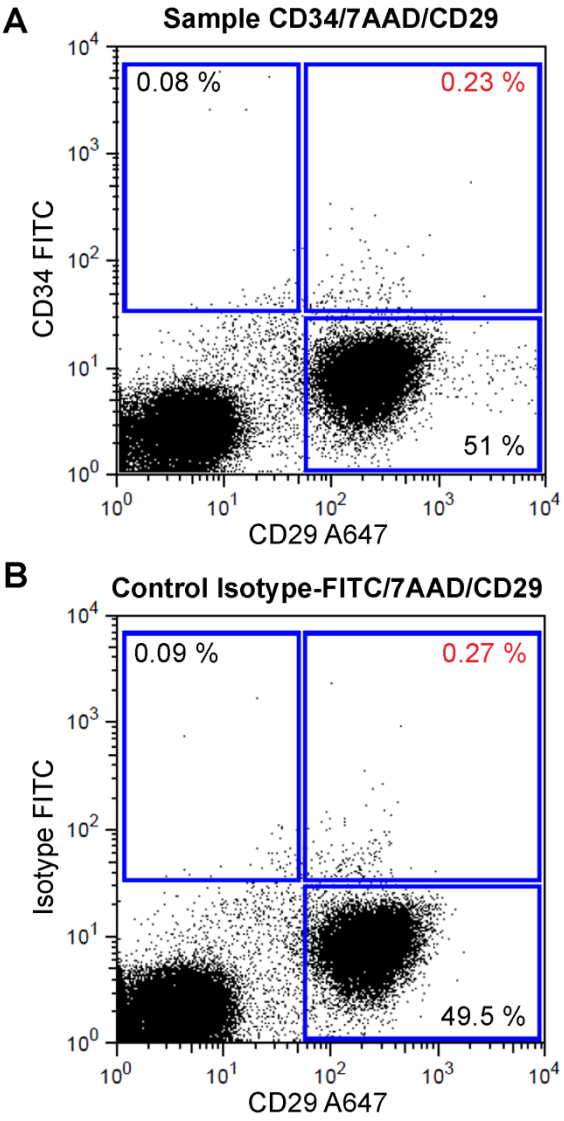

Esophageal epithelium does not contain a CD34 positive cell population.

Esophageal keratinocytes from C57/Bl6 mice were freshly isolated and stained for FACS analysis with 7AAD (viability marker), CD29-Alexa Fluor® 647 (basal keratinocyte marker) and, CD34-FITC or the FITC isotype control (**A** and **B**, respectively). 45000 events from viable single cells were acquired per sample. Comparison of the FITC-CD34 stained sample with the FITC-isotype control reveals no specific staining for CD34. Results shown are typical of three independent experiments.

Fig. S4

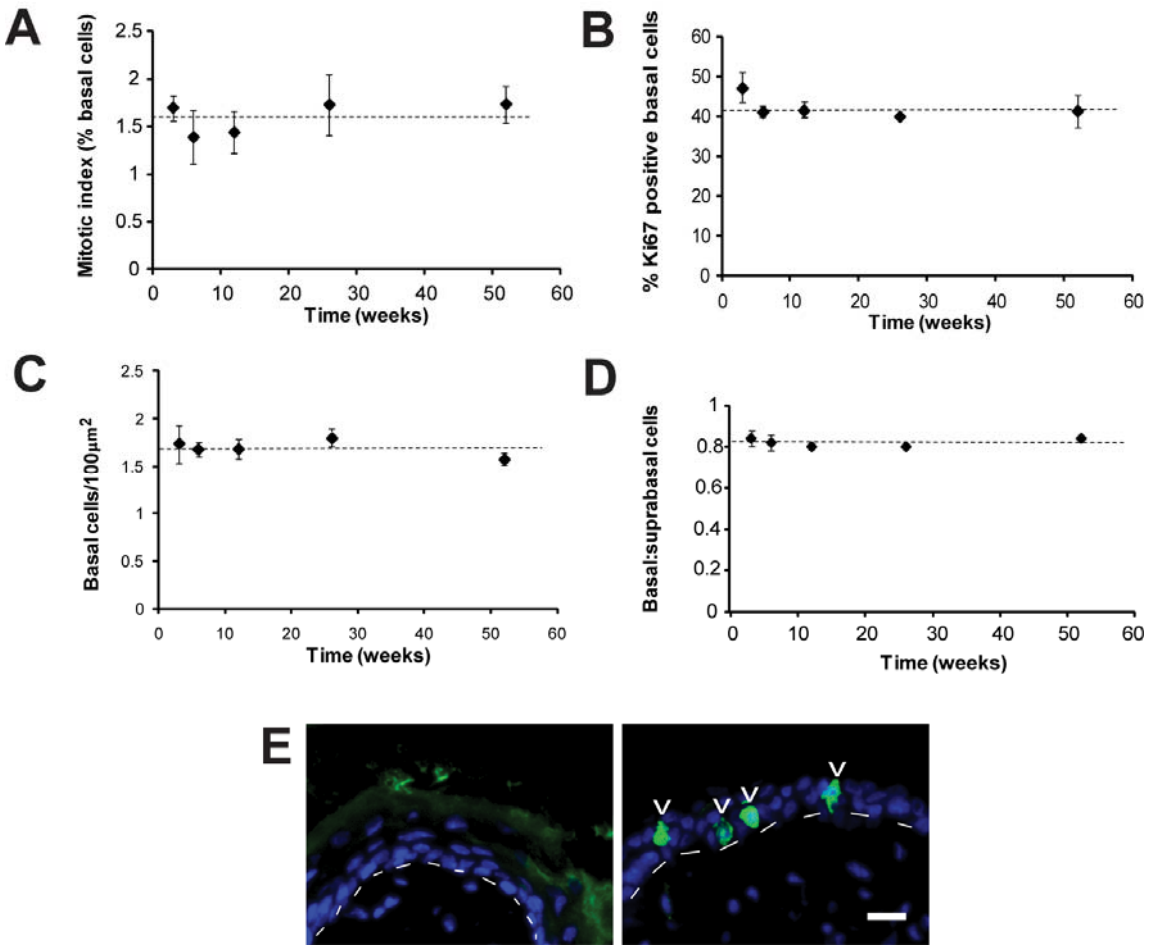

Homeostasis in EE over one year

A-D: Measurements of mitotic index (**A**), % Ki67 positive basal cells (**B**), basal cell density (cells/100µm^2) (**C**), and the ratio of basal cells: nucleated suprabasal cells (**D**) were performed, from at least 3 mice per time, dashed line shows the mean of all values at all time points, error bars indicate s.e.m. **E**: Activated Caspase 3 staining in EE. Left panel shows section of normal EE, right panel shows a UV irradiated explant culture as a positive control. Blue is Dapi, arrowheads indicate activated Caspase 3 positive cells (green), dashed line indicates basement membrane, scale bar 10µm. None of 30,000 basal cells from normal esophagus were positive for activated Caspase 3.

Fig. S5

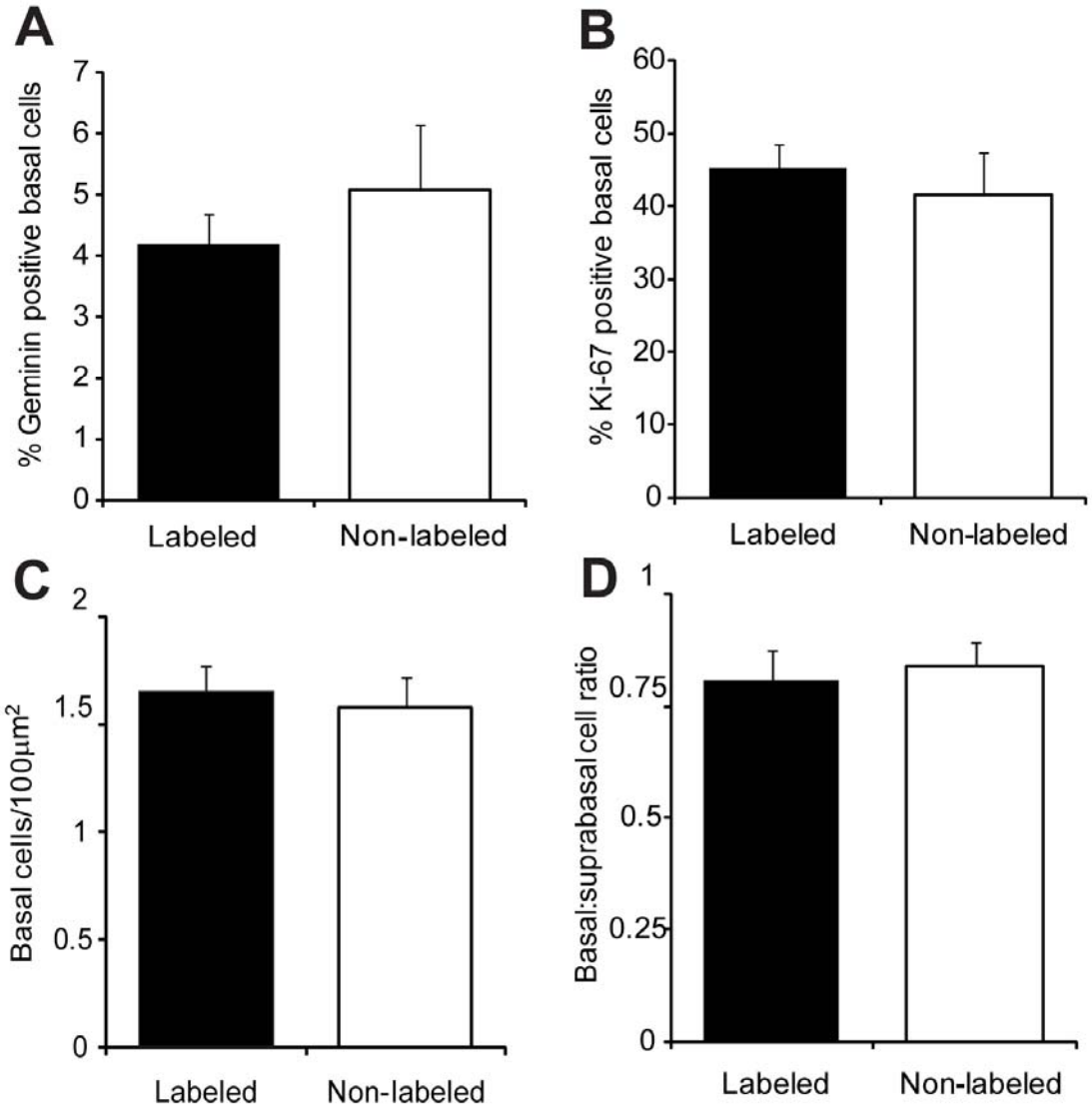

Representativeness of clonally labeled cells

A-D: Data from confocal imaging of labeled cells within clones and surrounding non labeled cells in EE wholemounts one year post-labeling. **A**, % Geminin positive basal cells; **B**, % Ki67 positive basal cells; **C**, basal cell density (cells/100μm^2); **D**, the ratio basal to nucleated suprabasal cells. Error bars indicate s.e.m. There was no statistically significant difference (P>0.2) when comparing labeled and unlabeled cells for any parameter by 2 tailed Student's t-test.

Fig. S6

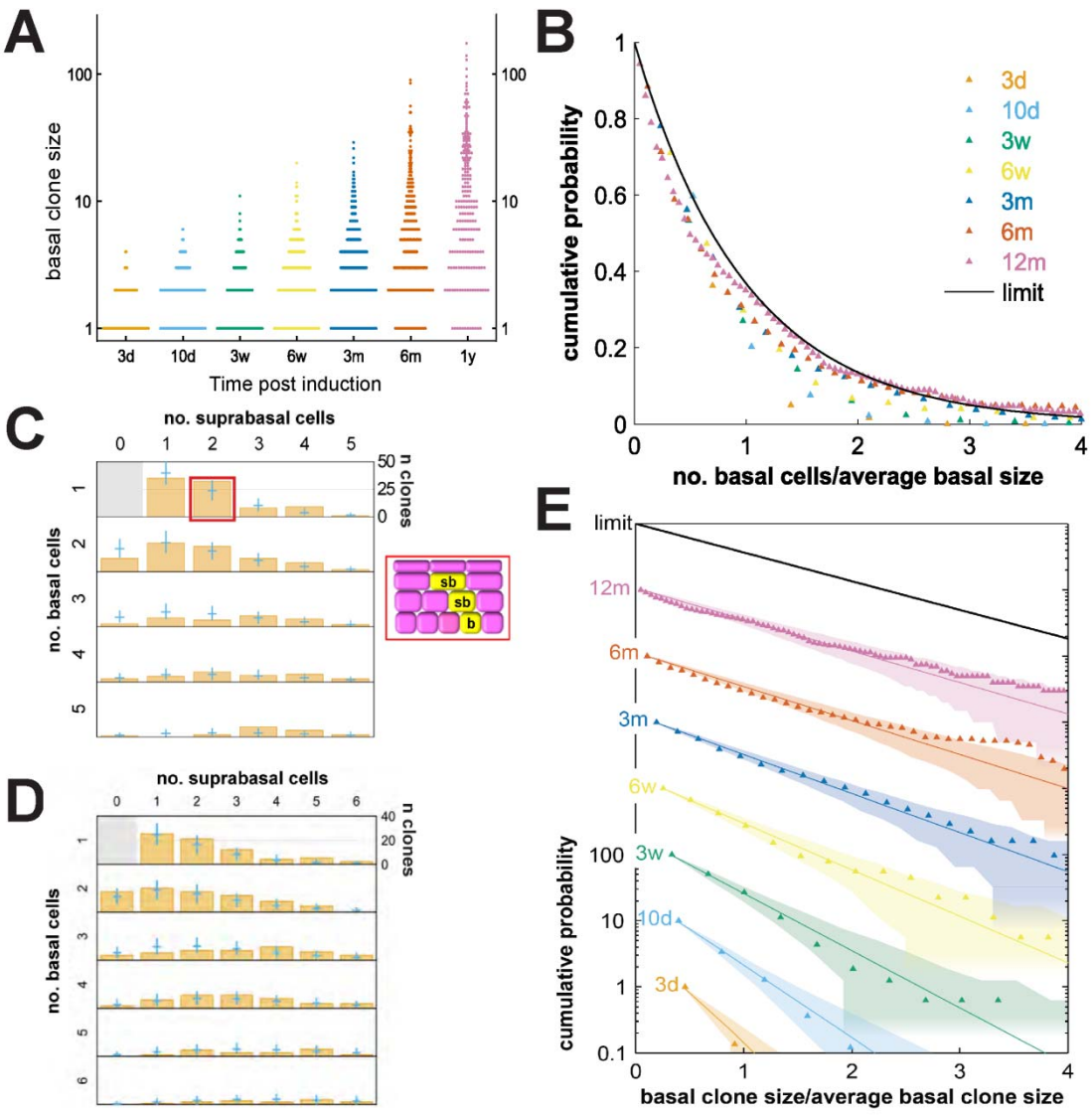

Clonal data and fit to model

A: Clone quantification. Clone size distribution (basal cells/clone) in a total of 1784 clones. Each point represents one clone, histograms are normalized so modal values are of equal width at each time.

B: Cumulative clone size distribution shows convergence onto scaling behavior at late times. The raw basal layer clone size distribution in panel A is reproduced here as the cumulative clone size distribution, $C_n(t)$, plotted as a function of n divided by the average clone size for each timepoint. The cumulative distribution $C_n(t)$ represents the probability of finding a surviving clone with a basal layer size larger than n. At times of 3 months or more post-induction, the data sets converge onto each other, a manifestation of long-term scaling behavior. Combined with the observed homeostatic nature of the turnover, such scaling behavior shows that the self-renewing progenitor cells function as a functionally equivalent population. The black curve denotes an exponential cumulative clone size distribution; the long-term behavior predicted for any strategy involving population asymmetric self-renewal including the model discussed here (*1-2*).

Fig S6 continued
C, D: Detailed clone size distribution at 30 (**C**) and 84 (**D**) days post-induction. Graph shows the joint distribution of basal and suprabasal cells in a total of 292 (**C**) and 489 (**D**) clones containing at least one basal layer cell, e.g. bar in red box in C indicates clones with 1 basal cell (b) and 2 suprabasal cells (sb), as shown in cartoon. The blue crosses show the prediction of the model represented in Fig. 2E with the 95% plausible interval indicated by vertical blue bars (see Supplementary Discussion and Results).

E: Cumulative basal layer clone size distribution, $C_n(t)$, as a function of size (number of cells) rescaled by the average for each time point, $n/\langle n(t)\rangle$ as in A, i.e. $C_n(t)$ denotes the probability of finding a clone with a size equal to, or larger than, $n/\langle n(t)\rangle$. Here we have presented the cumulative probability distribution on a logarithmic scale and, for clarity, we have separated consecutive time points by one decade. The points denote experimental data from panel A, and the lines represent the corresponding model predictions following the fit to the data with the parameters shown in Fig. 2E and 2F. The shaded regions represent estimates of the stochastic error due to finite sample size, indicating approximately one standard deviation (68%). In the long time limit, the model predicts that the distribution should tend to a simple exponential, $\exp(-n/\langle n(t)\rangle)$, (black line). The model shows good agreement with the experimental data at both short and long time points.

Fig S7

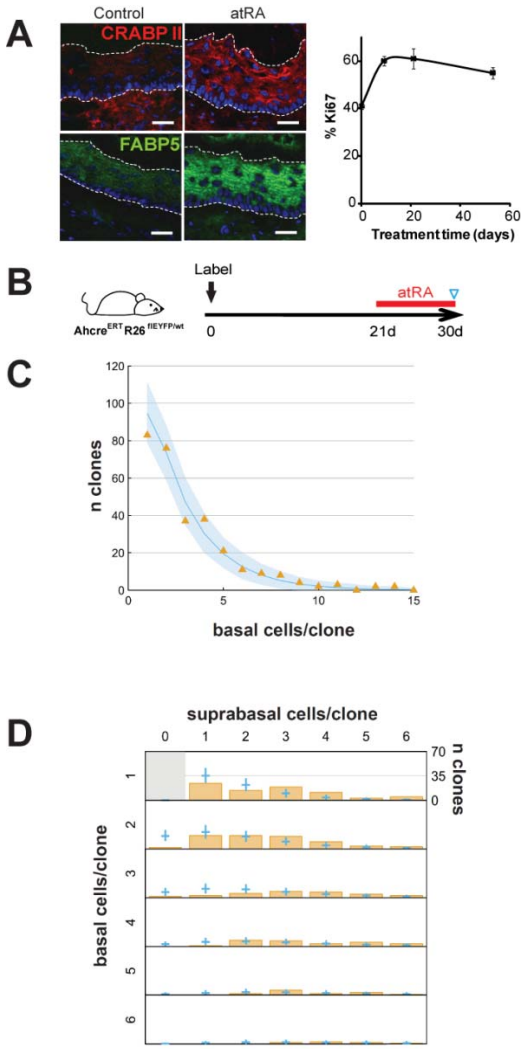

Response to atRA and second treatment protocol

A: Sections from control and treated mice, 24 hours after a single dose of atRA, stained for retinoid target genes CRABPII (red) or FABP5 (green), and DAPI (blue). Dotted lines enclose EE, note thickening in atRA samples. Scale bar 20 μm. Graph shows % Ki67 positive basal cells during atRA treatment.

B: To validate the model of the effects of atRA on EE shown in Fig. 3D, labeling was induced in Ahcre^{ERT}R26$^{flEYFP/wt}$ mice, which were then left untreated for 21 days after which they were treated with atRA on alternate days for 9 days. EE was then collected.

C: Number of basal cells per clone in EE treated as in B: orange triangles indicate experimental data, blue line indicates prediction of model shown in Figs 2F and 3D with 95% plausible interval. A total of 316 clones were scored in 3 mice.

D: Detailed clone size distribution of the same 316 clones, in orange. The blue crosses show the prediction of the model represented in Figs 2F and 3D with the 95% plausible interval indicated by vertical blue bars (see Supplementary text).

Fig. S8

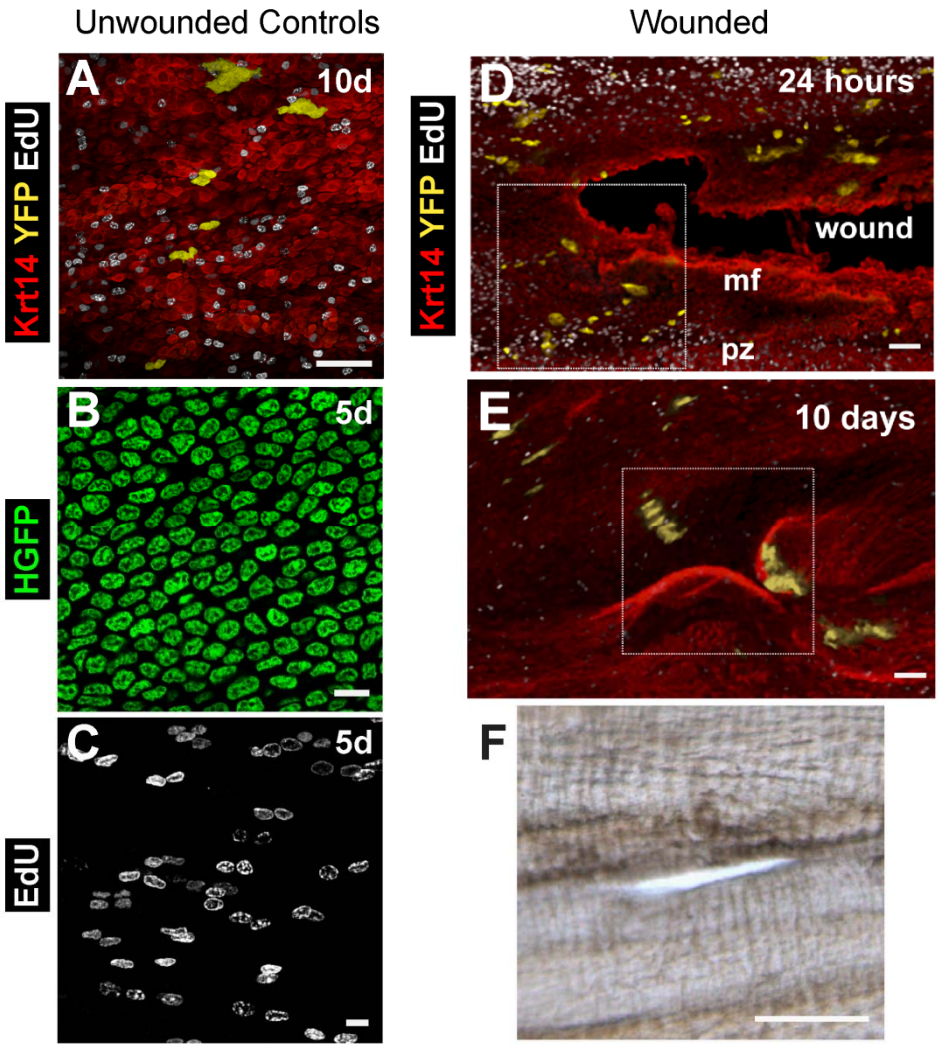

Controls for esophageal biopsy experiments and low power views of wound sites in biopsied mice

A-C Controls were anesthetized but did not undergo endoscopic biopsy, (see Fig. 4).

A: Clonal labeling control at 10 day post-wounding (compare with Fig. 4D). Ahcre^{ERT}R26$^{flEYFP/wt}$ mice were treated as shown in Fig. 4, column 1. EdU was given 1h before culling the animals and wholemounts were stained for YFP (yellow), EdU (white) and Keratin14 (Krt14, red). Scale bar 50 μm. **B**: HGFP dilution at 5 days post-wounding (compare with Fig. 4F). Rosa26^{M2rtTA}/TetO-HGFP mice were treated with doxycycline (DOX) for 4 weeks pre-biopsy and sampled as shown in Fig. 4, column 2. Wholemounts were imaged by confocal microscopy to detect endogenous HGFP fluorescence (green). Scale bar 10 μm. **C**: 24 hour EdU control at 5 day post-wounding (compare with Fig. 4I). Wild type animals were treated as shown in Fig. 4, column 3. EdU was given 24h before culling and wholemounts stained for EdU (greyscale). Scale bar 10 μm. Clone appearances, EdU staining and HGFP levels distant from the wound site in biopsied animals were similar to those in the unwounded controls.

D, E: Low power views of the wounds shown in Figs 4B and 4C respectively (regions imaged in Fig 4 indicated by white box), wholemounts were stained for YFP (yellow), EdU (white) and Keratin14 (red), scale bars 50μm.

F: Stereoscopic image of wound 2 days post-biopsy, scale bar 500μm.

Fig. S9

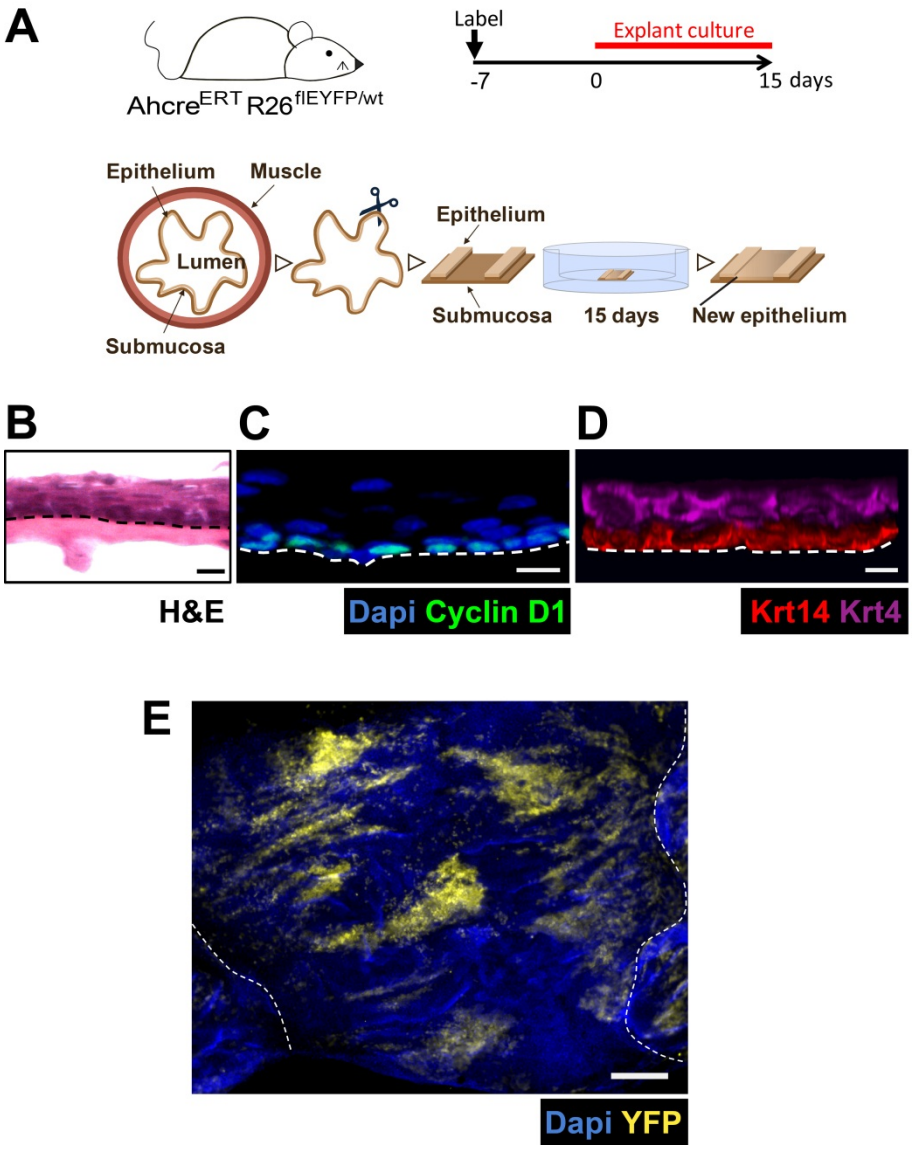

Progenitor fate switching in esophageal explant cultures.
A: Protocol for explant culture on submucosa: clonal labeling was induced in Ahcre^{ERT}R26$^{flEYFP/wt}$ mice 7 days prior tissue harvesting. Parallel strips of EE, with underlying submucosa, were laid on submucosa from unlabeled mice and cultured for a period of 15 days, over which new epithelium forms between the strips (see supplementary methods). **B-C**: cryosections of cultured epithelium, stained for hematoxylin and eosin (B) or Cyclin D1 (green) and DAPI (blue, C). Dashed line indicates basement membrane, scale bar 10µm. **D**: Rendered confocal Z stack of wholemount of cultured epithelium stained for the basal layer marker keratin 14 (red) and the suprabasal marker keratin 4 (purple), dotted line indicates basement membrane. Scale bar 10µm. **E**: Confocal z stack of epithelial wholemount preparation of explant culture. Yellow is YFP, blue is DAPI. Dashed lines indicate boundary of new epithelium formed in culture and the original strips of EE. Scale bar 200µm. Note labeled cells make a substantial contribution to the new epithelium, consistent with *in vivo* behavior (Fig. 4).

Fig. S10

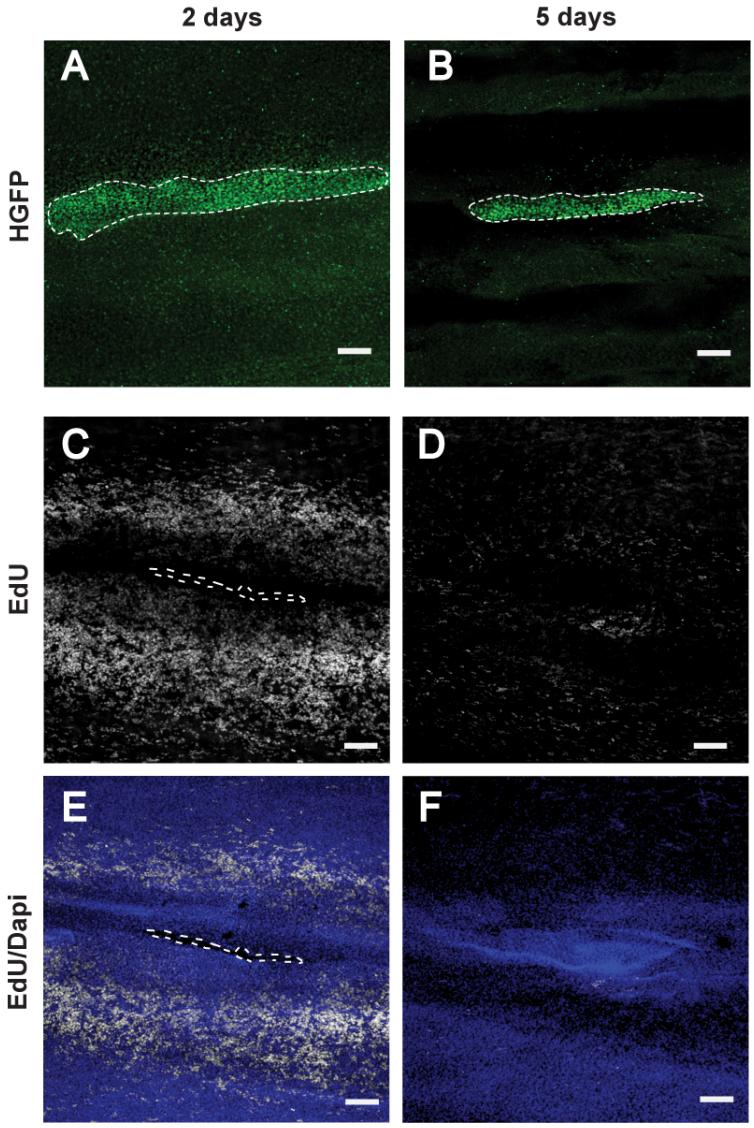

Epithelial proliferation at wound site.
A-B: Low power views of wounded EE in Rosa26^{M2rtTA}/TetO-HGFP mice treated with doxycycline (DOX) for 4 weeks pre-biopsy and sampled as shown in Fig. 4 column 2, at 2 days (**A**) and 5 days (**B**) post-biopsy, HGFP is green, note the epithelial defect has closed by 2 days in **A**. **C-F**: Low power view of wounded EE in wild type mice, treated with EdU 24 hours before culling, at 2 days (**C**, **E**) or 5 days (**D**, **F**) post-biopsy (Fig. 4, column 3). EdU is grayscale, dapi blue, dashed line in **C** and **E** indicates epithelial injury. Note HGFP retaining cells, encircled in dotted line in **A** and **B**, and EdU negative cells adjacent to the wound margin (**C-F**) correspond to the migratory front as indicated in Fig. 4B. Scale bars 100μm.

Fig. S11

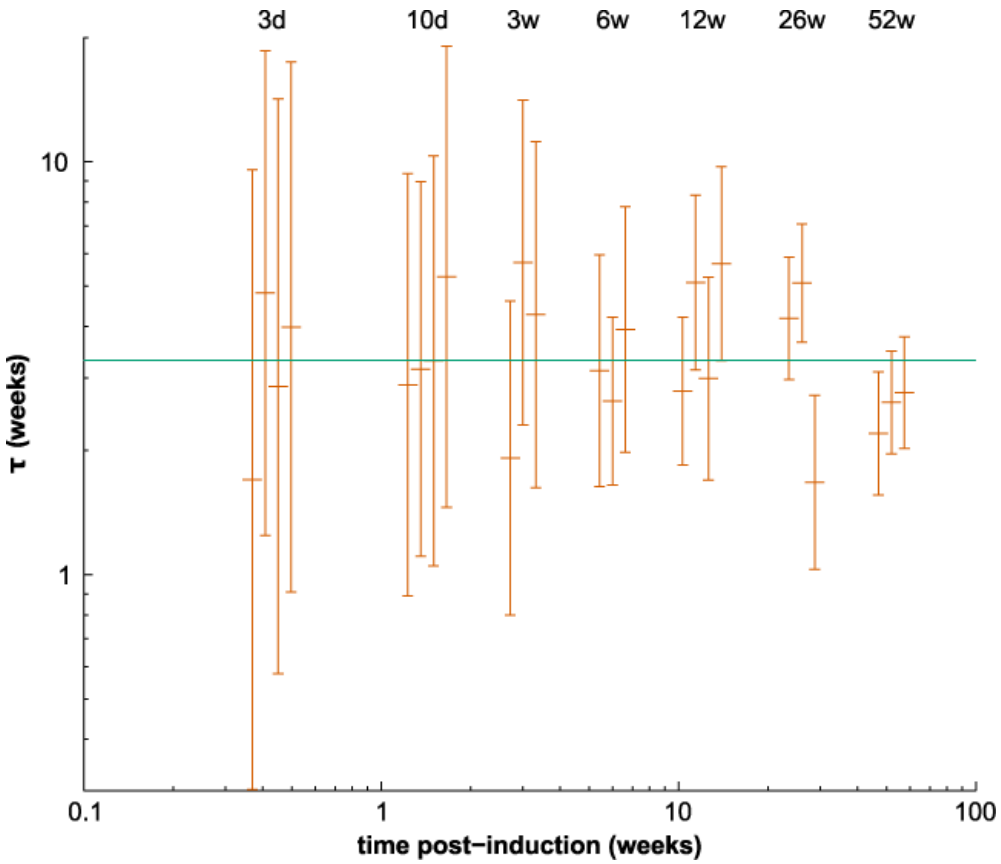

Estimation of τ from the basal clone size distribution of individual mice (data from Fig. S6, see supplementary theory). From the data from each mouse, we can separately estimate the combined parameter $\tau = \rho/\rho\lambda$. Here we plot $\log(\tau)$ with 68% (1σ) credible intervals for 28 mice, along with the combined average (and 1σ credible interval) in green from treating all mice as exactly identical.

Fig. S12

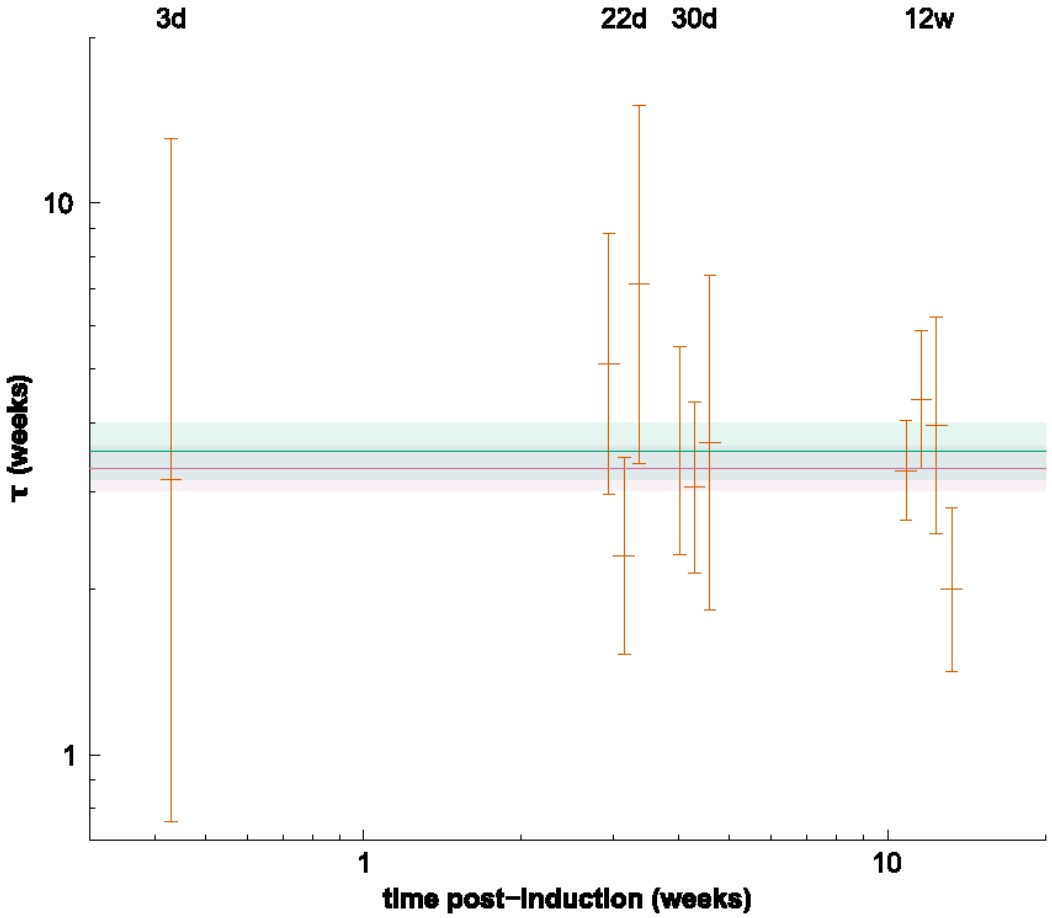

Estimation of τ from the detailed (basal and suprabasal) clone size distributions of individual mice (see Supplementary Theory).
$\log(\tau)$ with 68% (1σ) credible intervals is plotted for 11 mice, with the combined average in purple. The combined average from basal data in fig. S11 is reproduced in green.

Fig. S13

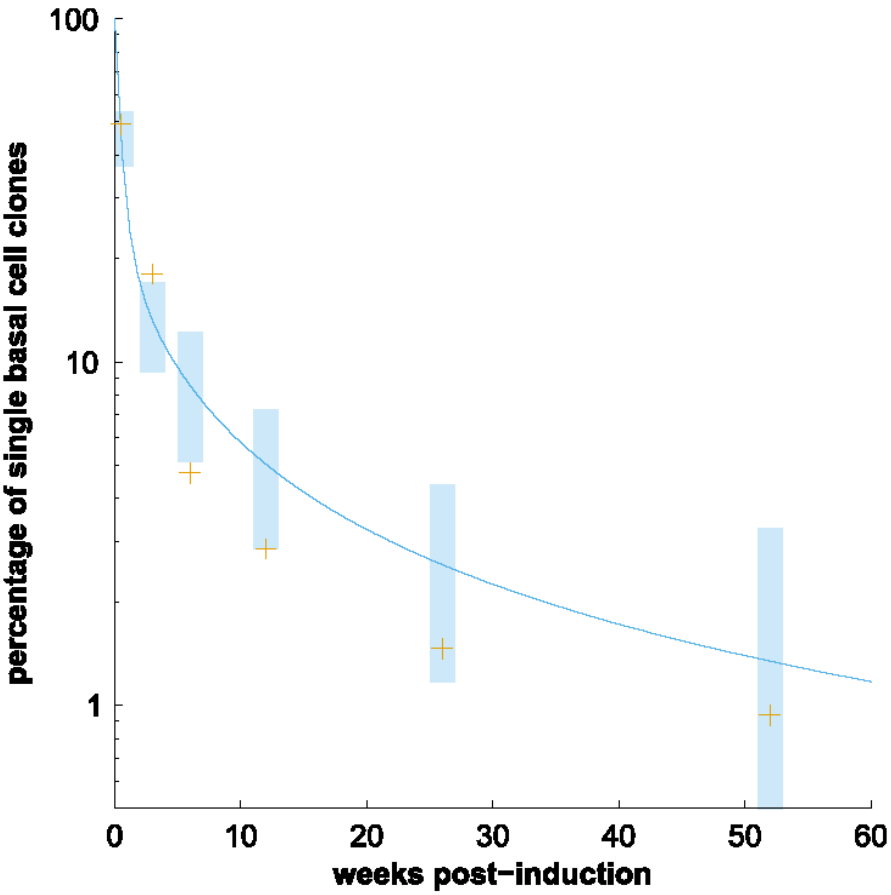

Relative frequency of clones with one basal cell and no suprabasal cells (see supplementary theory).
There is a very slow decay of the relative frequency of clones consisting of a single basal cell. Nevertheless, this is well accounted for by the model (Fig. 2F). Here we plot the observed relative frequency in orange, and in blue the model prediction (with 95% likelihood intervals arising from finite number of clones counted).

Table S1: Antibodies used for immunofluorescence

Antigen	Clone	Company	Cat No	Species	Dilution
GFP	-	Invitrogen	A11039	Chicken	1/500
K14	-	Covance	PRB-155P	Rabbit	1/1000
K4	6B10	Vector	VP-C399	Mouse	1/1000
CD45	30-F11	Biolegend	103102	Rat	1/200
CD3	17A2	eBiosciences	16-0032-82	Rat	1/100
CD34	RAM34	BD Biosciences	553731	Rat	1/100
Langerin	-	Santa Cruz	sc-22620	Goat	1/100
E-cadherin	24E10	Cell Signaling	3195	Rabbit	1/100
CyclinD1	SP4	Thermo Scientific	RM-9104	Rabbit	1/100
Active Caspase3	-	Abcam	Ab2302	Rabbit	1/100
Geminin	-	Gift Dr. MA Gonzalez	3988065	Rabbit	1/300
CRABPII	-	Proteintech	10225-1-AP	Rabbit	1/50*
FABP5	-	R&D systems	AF1476	Goat	1/50*

*Acetone/methanol fixation: all other samples were fixed with paraformaldehyde.

References

1. T. Tumbar *et al*., Defining the epithelial stem cell niche in skin. *Science* **303**, 359 (2004). doi:10.1126/science.1092436 Medline

2. N. Barker *et al*., Lgr5^{+ve} stem cells drive self-renewal in the stomach and build long-lived gastric units in vitro. *Cell Stem Cell* **6**, 25 (2010). doi:10.1016/j.stem.2009.11.013 Medline

3. N. Barker *et al*., Identification of stem cells in small intestine and colon by marker gene Lgr5. *Nature* **449**, 1003 (2007). doi:10.1038/nature06196 Medline

4. V. Jaks *et al*., Lgr5 marks cycling, yet long-lived, hair follicle stem cells. *Nat. Genet.* **40**, 1291 (2008). doi:10.1038/ng.239 Medline

5. E. Goetsch, The structure of the mammalian oesophagus. *Am. J. Anat.* **10**, 1 (1910). doi:10.1002/aja.1000100102

6. B. Messier, C. P. Leblond, Cell proliferation and migration as revealed by radioautography after injection of thymidine-H3 into male rats and mice. *Am. J. Anat.* **106**, 247 (1960). doi:10.1002/aja.1001060305 Medline

7. J. P. Marques-Pereira, C. P. Leblond, Mitosis and differentiation in the stratified squamous epithelium of the rat esophagus. *Am. J. Anat.* **117**, 73 (1965). doi:10.1002/aja.1001170106 Medline

8. J. P. Seery, F. M. Watt, Asymmetric stem-cell divisions define the architecture of human oesophageal epithelium. *Curr. Biol.* **10**, 1447 (2000). doi:10.1016/S0960-9822(00)00803-4 Medline

9. D. Croagh, W. A. Phillips, R. Redvers, R. J. Thomas, P. Kaur, Identification of candidate murine esophageal stem cells using a combination of cell kinetic studies and cell surface markers. *Stem Cells* **25**, 313 (2007). doi:10.1634/stemcells.2006-0421 Medline

10. J. Kalabis *et al*., A subpopulation of mouse esophageal basal cells has properties of stem cells with the capacity for self-renewal and lineage specification. *J. Clin. Invest.* **118**, 3860 (2008). Medline

11. D. Croagh, R. J. Thomas, W. A. Phillips, P. Kaur, Esophageal stem cells: A review of their identification and characterization. *Stem Cell Rev.* **4**, 261 (2008). doi:10.1007/s12015-008-9031-3 Medline

12. J. Dent, H. B. El-Serag, M. A. Wallander, S. Johansson, Epidemiology of gastro-oesophageal reflux disease: A systematic review. *Gut* **54**, 710 (2005). Medline

13. A. Jemal *et al*., Global cancer statistics. *CA Cancer J. Clin.* **61**, 69 (2011). doi:10.3322/caac.20107 Medline

14. T. Kanda, K. F. Sullivan, G. M. Wahl, Histone-GFP fusion protein enables sensitive analysis of chromosome dynamics in living mammalian cells. *Curr. Biol.* **8**, 377 (1998). doi:10.1016/S0960-9822(98)70156-3 Medline

15. K. Hochedlinger, Y. Yamada, C. Beard, R. Jaenisch, Ectopic expression of Oct-4 blocks progenitor-cell differentiation and causes dysplasia in epithelial tissues. *Cell* **121**, 465 (2005). doi:10.1016/j.cell.2005.02.018 Medline

16. H. J. Snippert *et al*., Intestinal crypt homeostasis results from neutral competition between symmetrically dividing Lgr5 stem cells. *Cell* **143**, 134 (2010). doi:10.1016/j.cell.2010.09.016 Medline

17. K. M. Braun *et al*., Manipulation of stem cell proliferation and lineage commitment: Visualisation of label-retaining cells in wholemounts of mouse epidermis. *Development* **130**, 5241 (2003). doi:10.1242/dev.00703 Medline

18. E. Clayton *et al*., A single type of progenitor cell maintains normal epidermis. *Nature* **446**, 185 (2007). doi:10.1038/nature05574 Medline

19. D. P. Doupé, A. M. Klein, B. D. Simons, P. H. Jones, The ordered architecture of murine ear epidermis is maintained by progenitor cells with random fate. *Dev. Cell* **18**, 317 (2010). doi:10.1016/j.devcel.2009.12.016 Medline

20. A. M. Klein, D. P. Doupé, P. H. Jones, B. D. Simons, Kinetics of cell division in epidermal maintenance. *Phys. Rev. E Stat. Nonlin. Soft Matter Phys.* **76**, 021910 (2007). doi:10.1103/PhysRevE.76.021910 Medline

21. A. M. Klein, B. D. Simons, Universal patterns of stem cell fate in cycling adult tissues. *Development* **138**, 3103 (2011). doi:10.1242/dev.060103 Medline

22. C. Lopez-Garcia, A. M. Klein, B. D. Simons, D. J. Winton, Intestinal stem cell replacement follows a pattern of neutral drift. *Science* **330**, 822 (2010). doi:10.1126/science.1196236 Medline

23. B. Chapellier *et al*., Physiological and retinoid-induced proliferations of epidermis basal keratinocytes are differently controlled. *EMBO J.* **21**, 3402 (2002). doi:10.1093/emboj/cdf331 Medline

24. C. A. Collins, F. M. Watt, Dynamic regulation of retinoic acid-binding proteins in developing, adult and neoplastic skin reveals roles for beta-catenin and Notch signalling. *Dev. Biol.* **324**, 55 (2008). doi:10.1016/j.ydbio.2008.08.034 Medline

25. C. S. Potten, T. D. Allen, The fine structure and cell kinetics of mouse epidermis after wounding. *J. Cell Sci.* **17**, 413 (1975). Medline

26. G. C. Gurtner, S. Werner, Y. Barrandon, M. T. Longaker, Wound repair and regeneration. *Nature* **453**, 314 (2008). doi:10.1038/nature07039 Medline

27. P. Martin *et al*., Wound healing in the PU.1 null mouse: Tissue repair is not dependent on inflammatory cells. *Curr. Biol.* **13**, 1122 (2003). doi:10.1016/S0960-9822(03)00396-8 Medline

28. A. Jacinto, A. Martinez-Arias, P. Martin, Mechanisms of epithelial fusion and repair. *Nat. Cell Biol.* **3**, E117 (2001). doi:10.1038/35074643 Medline

29. M. A. Gonzalez *et al*., Geminin is essential to prevent endoreduplication and to form pluripotent cells during mammalian development. *Genes Dev.* **20**, 1880 (2006). doi:10.1101/gad.379706 Medline

30. A. M. Klein, D. P. Doupé, P. H. Jones, B. D. Simons, Mechanism of murine epidermal maintenance: Cell division and the voter model. *Phys. Rev. E Stat. Nonlin. Soft Matter Phys.* **77**, 031907 (2008). doi:10.1103/PhysRevE.77.031907 Medline